Crystal Structure of (+)-δ-Cadinene Synthase from Gossypium arboreum and Evolutionary Divergence of Metal Binding Motifs for Catalysis

ARTICLE *in* BIOCHEMISTRY · JULY 2009

Impact Factor: 3.02 · DOI: 10.1021/bi900483b · Source: PubMed

8 AUTHORS, INCLUDING:

Luigi Di Costanzo
Rutgers, The State University of New Jersey
45 PUBLICATIONS **1,539** CITATIONS

SEE PROFILE

David J Miller
Cardiff University
24 PUBLICATIONS **357** CITATIONS

SEE PROFILE

Published in final edited form as:
Biochemistry. 2009 July 7; 48(26): 6175–6183. doi:10.1021/bi900483b.

Crystal Structure of (+)-δ-Cadinene Synthase from *Gossypium arboreum* and Evolutionary Divergence of Metal Binding Motifs for Catalysis,[†,‡]

Heather A. Gennadios[§], **Veronica Gonzalez**[#,Δ], **Luigi Di Costanzo**[§,¶,Δ], **Amang Li**[#], **Fanglei Yu**[#,•], **David J. Miller**[#], **Rudolf K. Allemann**[#,*], and **David W. Christianson**[*,§]

[§]Roy and Diana Vagelos Laboratories, Department of Chemistry, University of Pennsylvania, Philadelphia, PA 19104-6323

[#]School of Chemistry, Cardiff University, Park Place, Cardiff CF10 3AT, United Kingdom

[¶]Ben May Institute for Cancer Research, University of Chicago, Chicago, IL 60637

[•]NewChem Technologies Ltd. ·Bedson Building,· Kings Road, ·Newcastle upon Tyne, ·NE1 7RU, United Kingdom

Abstract

(+)-δ-Cadinene synthase (DCS) from *Gossypium arboreum* (tree cotton) is a sesquiterpene cyclase that catalyzes the cyclization of farnesyl diphosphate in the first committed step of the biosynthesis of gossypol, a phytoalexin that defends the plant from bacterial and fungal pathogens. Here, we report the X-ray crystal structure of unliganded DCS at 2.4 Å resolution and the structure of its complex with three putative Mg^{2+} ions and the substrate analogue inhibitor 2-fluorofarnesyl diphosphate (2F-FPP) at 2.75 Å resolution. These structures illuminate unusual features that accommodate the trinuclear metal cluster required for substrate binding and catalysis. Like other terpenoid cyclases, DCS contains a characteristic aspartate-rich motif D^{307}DTYD^{311} on helix D that interacts with Mg^{2+}_A and Mg^{2+}_C. However, DCS appears to be unique among terpenoid cyclases in that it does not contain the "NSE/DTE" motif on helix H that specifically chelates Mg^{2+}_B, which is usually found as the signature sequence (**N, D**)D(L, I, V)X(**S, T**)XXX**E** (boldface indicates Mg^{2+}_B ligands). Instead, DCS contains a second aspartate-rich motif, D^{451}DVAE^{455}, that interacts with Mg^{2+}_B. In this regard, DCS is more similar to the isoprenoid chain elongation enzyme farnesyl diphosphate synthase, which also contains two aspartate-rich motifs, rather than the greater family of terpenoid cyclases. Nevertheless, the structure of the DCS-2F-FPP complex shows that the structure of the trinuclear magnesium cluster is generally similar to that of other terpenoid cyclases despite the alternative Mg^{2+}_B-binding motif. Analyses of DCS mutants with alanine substitutions in the D^{307}DTYD^{311} and D^{451}DVAE^{455} segments reveal the contributions of these segments to catalysis.

Antimicrobial natural terpenoid products known as phytoalexins are generated by tree cotton (*Gossypium arboreum*, indigenous to India and Pakistan) in response to threats from bacterial or fungal pathogens (1-2). These products are classified as secondary metabolites and are

[†]This work was supported by National Institutes of Health grant GM56838 (D.W.C.), BBSRC grants 6/B17177 (R.K.A.) and BB/G003572/1 (R.K.A), EPSRC grant EP/D06958/1 (R.K.A), Royal Society grant 2007R2 (R.K.A.), and Cardiff University.

[‡]The atomic coordinates of unliganded (+)-δ-cadinene synthase and its complex with 2-fluorofarnesyl diphosphate have been deposited in the Protein Data Bank (www.rcsb.org) with accession codes 3G4D and 3G4F, respectively.

[Δ]These authors made equal contributions to this study.

[*]To whom correspondence should be addressed: DWC: Tel: 215-898-5714. Fax: 215-573-2201. Email: chris@sas.upenn.edu; RKA: Tel: +44 29 2087 9014. Fax: +44 29 2087 4030. Email: allemannrk@cardiff.ac.uk.

therefore non-essential for plant viability; however, they mediate important interactions between plants and their environments (3). The 64 kDa sesquiterpenoid cyclase (+)-δ-cadinene synthase (DCS, isozyme XC1; SWISS-PROT accession code Q39761) catalyzes the formation of (+)-δ-cadinene from farnesyl diphosphate (FPP)[1], which is the first committed step in the biosynthesis of the triterpene phytoalexin gossypol (4-7) (Figure 1). Gossypol is the predominant terpenoid found in the glands of aerial tissues and in epidermal cells of roots and is the major defense metabolite generated in cotton plants. Notably, gossypol has also been studied as a male contraceptive drug (8,9) and as a potential cancer chemotherapeutic agent (10-13).

The catalytic mechanism of DCS (Figure 1) is believed to be initiated by the metal-dependent isomerization of FPP to yield (3*R*)-nerolidyl diphosphate (NPP), which then undergoes metal-dependent re-ionization after achieving a cisoid conformation to yield an allylic cation-pyrophosphate anion pair. The first carbon-carbon bond forming reaction in the cyclization cascade is electrophilic attack of C1 at the C10-C11 •-bond, which is followed by a 1,3-hydride shift from C2 to C11 to form the 3*Z*, 7*E*-germacryl cation. Subsequent electrophilic attack of the allylic C2 carbocation at the C7-C8 π-bond generates the cadinyl cation, which is ultimately quenched by deprotonation at C7 to form (+)-δ-cadinene (5,14,15). Recent gas-phase quantum chemical calculations support the viability of the postulated mechanism for the formation of the bicyclic cadinyl skeleton (16). Significantly, DCS is a “high-fidelity” terpenoid cyclase since it generates (+)-δ-cadinene nearly exclusively (>98 %) (see Supporting Information) (15). This contrasts with the output of more promiscuous cyclases such as γ-humulene synthase, which generates a total of 52 sesquiterpenoid products from substrate FPP (17).

Based on sequence alignments with other terpenoid cyclases, the amino acid sequence of DCS (5) indicates that helix D of the catalytic domain contains the aspartate-rich segment D^{307}DTYD^{311}, which is the signature **D**DXX(X)**D/E** metal binding motif common to

[1]Abbreviations:

APS Advanced Photon Source

ATAS *Aspergillus terreus* aristolochene synthase

BME β-mercaptoethanol

DCS (+)-δ-cadinene synthase

FPP farnesyl diphosphate

2F-FPP 2-fluorofarnesyl diphosphate

10F-FPP 10-fluorofarnesyl diphosphate

FPPS farnesyl diphosphate synthase

GC-MS gas chromatography-mass spectroscopy

NPP nerolidyl diphosphate

PEG polyethylene glycol

terpenoid cyclases (boldface residues typically coordinate to Mg^{2+} ions). However, DCS does not contain the characteristic "NSE/DTE" metal binding motif on helix H, which is usually found as the signature sequence (**N, D**)D(L, I, V)X(**S, T**)XXX**E** that specifically chelates Mg^{2+}_B (18,19); (boldface indicates Mg^{2+}_B ligands; occasionally, glycine is observed in place of (**S, T**), in which case an additional water molecule may coordinate to Mg^{2+}_B (20)). Instead, DCS contains a second aspartate-rich motif $D^{451}DVAE^{455}$. Ordinarily, the NSE/DTE motif distinguishes a terpenoid cyclase from a terpenoid synthase that catalyzes an isoprenoid chain elongation reaction, such as farnesyl diphosphate synthase (21-23). Thus, the metal coordination polyhedra required for substrate binding and catalysis distinguish DCS from other terpenoid cyclases (24-27).

We recently reported the crystal structures of aristolochene synthase from *A. terreus* complexed with various fluorinated farnesyl diphosphate analogues (28). These structures reveal conformational changes that the enzyme can undergo upon complexation with substrate analogues and metal ions, thereby exemplifying the utility of fluorinated isoprenoid derivatives in the study of structure-function relationships. Here, we report the X-ray crystal structure of DCS from *G. arboreum* and the structure of its complex with 2-fluorofarnesyl diphosphate (2F-FPP). Additionally, we present product distribution and kinetic data for DCS mutants with aspartate->alanine and glutamate->alanine substitutions in the $D^{307}DTYD^{311}$ and $D^{451}DVAE^{455}$ segments. These results taken together illuminate aspects of metal binding in an unusual terpenoid cyclase active site and provide inferences regarding conformational changes that may occur upon substrate binding and catalysis.

Materials and Methods

Synthesis of fluorinated FPP analogues

The substrate analogue 2F-FPP was prepared from geranyl acetone as previously described (29). The synthesis of 10F-FPP is outlined in the Supporting Information.

Expression and purification

Plasmid pXC1 (a kind gift from Dr Xiao-Ya Chen) containing the cDNA for DCS (5) was modified to introduce NcoI and BamHI sites at the 5′ and 3-ends respectively using the primers 5′-CATGCCATGGCTTCACAAGTTTCTCAAATGCC-3′ and 5′-CGGGATCCTCAAAGTGCAATTGGTTCAATGAGC-3′ and then inserted into pET 21d (Stratagene). Rosetta2(DE3)pLysS cells were then transformed with this plasmid. Six single colonies of transformed cells were added to 5 mL of YT medium containing 50 μg/mL ampicillin and 34 μg/mL chloramphenicol. Cultures were grown overnight at 37 °C with shaking. The 5 mL overnight cultures were used to inoculate 6 × 500 mL of sterile YT medium containing the appropriate antibiotics. Cells were incubated at 37 °C with shaking until the absorbance at 600 nm was between 0.5-0.8. Expression was induced with 500 μM IPTG and incubated at 37 °C with shaking for 3 hours. The cells were pelleted by centrifugation for 10 minutes at 6000 rpm and the supernatant was decanted and discarded. The cell pellet was stored at -20 °C until needed.

Pellets were thawed and resuspended in 25 mL of cell lysis buffer (20 mM Tris (pH 8.0), 5 mM EDTA, 5 mM β-mercaptoethanol (BME)). Cells were lysed by sonication (50% duty cycle, 50% output) using 3 × 2 minute pulses. The lysed cells were centrifuged at 16,000 rpm for 30 minutes and the supernatant was discarded (DCS remained solely in the insoluble portion). The pellets were resuspended in 150 mL of fresh lysis buffer and titrated on ice with light stirring with 0.1 M NaOH until the solution became clear (~ pH 11.6). The solution was stirred on ice for 30 minutes. The pH was then lowered to pH 7.5 with 0.1 M HCl and BME added to

a final concentration of 5 mM. The resulting solution was stirred on ice for 30 min and centrifuged at 16,000 rpm. DCS remained in the soluble supernatant.

A 5 mL HiTrap DEAE Fast Flow column (GE Biosciences) was utilized. The column was washed with 5-10 column volumes of lysis buffer. The protein was loaded onto the column and washed with another 5-10 column volumes of lysis buffer. A linear gradient ranging from 0 - 600 mM NaCl was applied to the column and the protein eluted with ~240 mM NaCl. Fractions containing protein were analyzed on an SDS-PAGE gel and pooled together. The protein was concentrated to ~6 mL total volume. A 26/60 Superdex 200 size exclusion column (GE Biosciences) was washed with one column volume of buffer (20 mM Tris (pH 8.0), 50 mM NaCl, 5 mM BME). The protein eluted in two different peaks. The first peak eluted at the void volume for the column, indicating that the protein in this peak was most likely composed of soluble aggregates. The second peak corresponded to the molecular weight of the DCS monomer (64 kD). The fractions were analyzed by SDS-PAGE and those corresponding to the DCS monomer from the size exclusion chromatogram were pooled and concentrated to a final protein concentration of ~10 mg/mL. The estimated purity was > 85%.

Site-directed mutagenesis of recombinant DCS cDNA is described in the Supporting Information. The expression and purification of mutant DCS enzymes was identical to that described above for wild-type DCS except that instead of using size exclusion chromatography in the final step, protein was purified using a Resource Q column (GE Healthcare, 6 ml) eluting with a NaCl gradient from 0-1 M over 15 column volumes with enzymes eluting between 200 and 500 mM NaCl.

Steady-state kinetic parameters of the mutants were measured at 25 °C using a radiochemical assay modified slightly from that used to determine kinetic parameters for the sesquiterpene cyclase aristolochene synthase (30). Assays (250 μL final volume) were initiated by addition of purified DCS solution (0.5 μM) to 1-200 μM [1-^{3}H]-farnesyl diphosphate (240000 dpm/nmol) in 25 mM HEPES, 15 mM $MgCl_2$, 5 mM DTT (pH 7.5). After incubation for 12 or 15 min, reactions were stopped by addition of 100 mM EDTA and overlayed with hexane (1 mL). After vortexing for 10 seconds, the hexane was removed and the sample extracted with hexane in the same way (2 × 1 mL). The pooled fractions were passed through a short column containing approximately 500 mg silica into a scintillation vial containing 15 mL of Ecoscint and analyzed by scintillation counting.

Inhibition assays were performed in identical fashion except for the addition of 2F-FPP at concentrations ranging from 0-120 μM. The IC_{50} value was calculated from inhibition assays at [FPP] = 8 μM fitting the data (corrected using negative controls) to the equation $V_i/V_0 = 1/(1+[I]/IC_{50})$ and the values for K_M and k_{cat} were calculated by fitting the data to the equation $v = (k_{cat}[E_{total}][S])/(K_M + [S])$ using Systat Sigmaplot 10.

Incubation of DCS with FPP

The DCS solution (25 μl, 70 ΓM) was diluted with 500 μL buffer consisting of 25 mM HEPES, 5 mM DTT, 15 mM $MgCl_2$ (pH 7.5). The assay solution was gently mixed as 10 mM FPP (25 μL) was added followed by pentane (100 μL). After incubation for 24 h at 25 °C the olefin products were extracted with pentane (3 × 1 mL). This solution was passed through a short pad of silica gel (~500 mg) and analyzed by gas chromatography-mass spectrometry (GC-MS). The GC-MS experiments were performed on a Hewlett Packard 6890 GC fitted with a J&W scientific DB-5MS column (30 m × 0.25 mm internal diameter) and a Micromass GCT Premiere detecting in the range *m/z* 50-800 in EI^+ mode with scanning once a second with a scan time of 0.9 sec. Injections were performed in split mode (split ratio 5:1) at 50 °C. Chromatograms were begun with an oven temperature of 50 °C rising at 4 °C min^{-1} for 25 min (up to 150 °C) and then at 20 °C min^{-1} for 5 min (250 °C final temperature).

Crystallization and structure determination

Crystals of DCS were grown by the hanging drop vapor diffusion method. Briefly, a drop containing 5 μL protein solution (10 mg/mL DCS, 20 mM Tris (pH 8.0), 2 mM $MgCl_2$, 5 mM BME) and 5 μL precipitant solution (100 mM Tris (pH 7.5), 200 mM Li_2SO_4, 15-17% polyethylene glycol (PEG) 4000, 100 mM $BaCl_2 \cdot 2H_2O$) was suspended over a reservoir of 600 μL precipitant solution. Crystals of DCS grew within 1-2 days with dimensions 0.2 mm × 0.2 mm × 0.1 mm. Crystals were soaked in a precipitant solution containing 5 mM 10-fluorofarnesyl diphosphate (10F-FPP) for 16 hours and were cryoprotected in a similar precipitant solution containing 5 mM 10F-FPP, 5 mM $MnCl_2$, and 25% glycerol prior to being flash cooled in liquid nitrogen. Crystals diffracted X-rays to 2.4 Å resolution at the Advanced Photon Source (APS) (Argonne National Laboratory, Argonne, IL), NE-CAT beamline 24-ID-C, and belonged to space group $P2_13$ with unit cell parameters $a = b = c = 158.20$ Å, with two molecules in the asymmetric unit (solvent content = 52%). Data were processed using HKL2000 (31). Initial phases were determined by molecular replacement using Phaser (32), with *Nicotiana tabacum* 5-epi aristolochene synthase (PDB accession code 5EAT, 48% amino acid sequence identity) (33) less all metal ions, ligands, and solvent molecules, used as a search probe. Iterative cycles of refinement and model building were performed with CNS (34), O (35), and Coot (36) to improve the structure as monitored by R_{free}. Strict non-crystallographic symmetry (NCS) constraints were used during the initial stages of refinement and then relaxed into appropriately weighted restraints as indicated by R_{free} as refinement progressed. The inspection of electron density maps did not reveal the presence of 10F-FPP, which was present in the crystal soaking buffer. Atomic displacement parameters were refined using the default restraints employed in the program PHENIX (37). Refinement was completed using PHENIX (37), and PROCHECK (38) was used to validate the structural model. Atomic coordinates of solvent molecules, two glycerol molecules, and two BME molecules were added during the last stages of refinement, and a disulfide linkage was observed between C408 and C447. One residue, F458 in monomer B, was found to adopt a disallowed backbone conformation; this residue is located in a partially disordered loop between helices H and Hα-1 and is characterized by moderately weak electron density. Disordered segments were excluded from the final model. Data collection and refinement statistics are listed in Table 1.

To determine the structure of the complex with 2-fluorofarnesyl diphosphate (2F-FPP), crystals of unliganded DCS were gradually transferred to a stabilizing solution containing 100 mM Tris (pH 7.5), 200 mM Li_2SO_4, 17-19% PEG 4000, 2 mM 2F-FPP and allowed to soak for 16 hours. Crystals were slowly cryoprotected with stabilizing solution containing 2 mM $MnCl_2$ and 25% glycerol and then flash cooled with liquid nitrogen. Data were collected to 2.75 Å resolution at the SER-CAT beamline 22-ID-D, at APS. Crystals were isomorphous with those of the unliganded enzyme. Data collection and refinement were performed as described for the structure determination of unliganded DCS. Atomic coordinates of solvent molecules and 2F-FPP were added during the last stages of refinement. Data collection and refinement statistics are reported in Table 1.

Results

Inhibition of DCS by 2F-FPP

Incubation of DCS with 2F-FPP does not lead to the generation of any detectable pentane-extractable products by GC-MS even after extended incubation times. When incubated with the enzyme and 10 μM FPP, 2F-FPP exhibits an IC_{50} value of approximately 30 μM. However, despite repeated attempts to determine its mode of inhibition, no consistent behavior in this regard could be determined (see Supporting Information). Similar complexity in the inhibition pattern of terpene synthases by substrate analogues is also observed for limonene synthase and

bornyl diphosphate synthase (39). Regardless, we conclude that 2F-FPP is sufficiently stable for X-ray crystallographic studies with DCS (*vide infra*).

Structure of unliganded DCS

The crystal structure of DCS is only the second to be reported to date for a plant sesquiterpene cyclase; the first was that of tobacco 5-epi-aristolochene synthase (33). Since the structure of DCS determined from crystals soaked with 10F-FPP contains no bound ligand, this structure provides a view of the unliganded enzyme. The structures of the two DCS monomers in the asymmetric unit are essentially identical; the r.m.s deviation of 499 Cα atoms between monomers A and B is 0.68 Å. The buried surface area between monomers A and B is 637 $Å^2$, which is too small to indicate a biologically relevant dimer. This is consistent with gel permeation chromatography experiments showing that DCS functions as a monomer in solution (7). The root mean square (r.m.s.) deviations of 499 Cα atoms between DCS and 5-epi-aristolochene synthase (the search probe used in molecular replacement calculations) is 1.0 Å.

The C-terminal catalytic domain of DCS adopts the α-helical class I terpenoid synthase fold (Figure 2) first observed for avian farnesyl diphosphate synthase (21). This fold was subsequently observed in sesquiterpene cyclases such as pentalenene synthase (40), 5-epi-aristolochene synthase (33), and monoterpene cyclases such as bornyl diphosphate synthase (41); structure-function relationships in the greater family of terpenoid cyclases have been reviewed (24-27,42). Six α-helices frame the ~18 Å-deep active site cleft, and helices D and H are on opposite walls of this cleft. Analysis of the crystal structure confirms that the first aspartate-rich motif (D^{307}DTYD^{311}) is located on the C-terminal end of helix D and the second aspartate-rich motif (D^{451}DVAE^{455}) is located at the C-terminal end of helix H. The non-catalytic N-terminal domain of DCS adopts an α-helical fold comparable to that of a class II terpenoid synthase, as first noted (25) for the N-terminal domain of 5-epi-aristolochene synthase (33).

In monomers A/B, the N-termini (M1-K24/M1-P29) and loop segments K42-I44/K42-D45, F460-D464/F460-D464, and G530-T534/Y533-V536 are disordered and excluded from the final model. Apart from the K42-I44/K42-D45 segment, each of these disordered segments is adjacent to the active site in the C-terminal domain. In some but not all unliganded terpenoid cyclases, one or more disordered polypeptide segments flank the mouth of the active site but become ordered upon the binding of magnesium ions and substrate analogues or products. Such structural transitions lead to a closed active site conformation that sequesters the substrate and reactive carbocation intermediates from bulk solvent, as recently reviewed (26,27).

Structure of the DCS-2F-FPP complex

The overall conformation of DCS in its complex with the substrate analogue inhibitor 2F-FPP and 3 metal ions is similar to that of unliganded DCS (Figure 2), with an r.m.s. deviation of 0.28 Å for 514 Cα atoms between the structures of liganded and unliganded monomer A, and an r.m.s. deviation of 0.50 Å for 494 Cα atoms between the structures of liganded and unliganded monomer B. The binding of 2F-FPP does not rigidify disordered polypeptide segments: the N-termini (M1-K24) and loop segments K42-I44, F460-D464, and G530-T534 remain disordered in each monomer. This contrasts with structural changes observed upon ligand binding to fungal terpenoid cyclases, in which significant active site conformational changes result in active site closure with r.m.s. deviations of ~1.5 Å for Cα atoms between liganded and unliganded structures (19,43). Intriguingly, overall conformational changes between liganded and unliganded catalytic domains of plant cyclases are somewhat smaller than those observed for fungal cyclases. For example, although significant local structural changes are triggered by ligand binding to the active site of bornyl diphosphate synthase, the

r.m.s. deviation of 306 Cα atoms in the catalytic domain is only 0.61 Å (41). Ligand binding to the active site of 5-epi-aristolochene synthase results in partial ordering of loop residues flanking the active site, but otherwise only minimal overall structural changes result to yield an r.m.s. deviation of 0.43 Å for 308 Cα atoms in the catalytic domain (33). Thus, it is possible that overall conformational changes triggered by ligand binding to the active sites of plant cyclases are somewhat attenuated in comparison with fungal cyclases, perhaps due to the presence of the additional N-terminal domain in the plant cyclases.

The binding of 2F-FPP to monomer A and monomer B is generally similar (Figure 3) and the overall r.m.s. deviation between monomer A and monomer B is 0.43 Å for 515 Cα atoms. The diphosphate group of 2F-FPP engages in few hydrogen bond interactions: in monomer A, the terminal diphosphate group of 2F-FPP accepts a hydrogen bond from R448, and the prenyl phosphoester oxygen donates a hydrogen bond to a water molecule that, in turn, accepts a hydrogen bond from R270. In monomer B, the corresponding interactions of the 2F-FPP diphosphate group are too long (3.5-3.6 Å) to be considered hydrogen bond interactions.

A Bijvoet difference Fourier map calculated with anomalous scattering data collected at λ = 1.0 Å does not reveal any peaks corresponding to bound Mn^{2+} or Ba^{2+} ions (data not shown; recall that DCS crystals were prepared in 100 mM $BaCl_2$ and cryoprotected in 2 mM $MnCl_2$). Although we cannot rule out low occupancy binding of Mn^{2+} or Ba^{2+}, we conclude that the 3 electron density peaks observed in the active site adjacent to the aspartate-rich segments with peak heights of 12.5σ, 7.4σ, and 11.3σ, correspond to putative Mg^{2+}_A, Mg^{2+}_B, and Mg^{2+}_C ions, respectively. Importantly, the binding sites of these ions correspond to the binding sites of magnesium ions in other terpenoid synthases (Figure 4). Curiously, several residues that interact with the putative Mg^{2+} ions in DCS do so with separations that are too long to be considered inner sphere metal coordination interactions (average separation = 2.7 Å). While such interatomic separations are more consistent with hydrogen bond interactions than inner sphere metal coordination interactions - indeed, we considered that the potential metal binding sites could be occupied by water molecules instead of Mg^{2+} ions - we ultimately disfavored the interpretation of solvent molecules due to the electron density peak heights observed for the 3 putative Mg^{2+} ions. If these peaks correspond to Mg^{2+} ions, then perhaps their interactions become closer and stronger upon the transition from an “open” to a “closed” active site conformation.

Mutagenesis of the aspartate-rich motifs

In order to further probe the role of the aspartate-rich motif $D^{307}DTYD^{311}$ on helix D that interacts with the putative Mg^{2+}_A and Mg^{2+}_C ions, the D307A, D308A and D311A mutants have been produced and purified using a protocol similar to that used for the purification of wild-type DCS. All mutant proteins generate δ-cadinene as the sole product as determined by GC-MS (see Supporting Information). For the cyclization of FPP by D308A DCS, $K_M = 43 \pm 16$ μM and $k_{cat} = 0.012 \pm 0.001$ s^{-1}. In comparison, the cyclization of FPP by wild-type DCS yields $K_M = 3.2 \pm 0.5$ μM and $k_{cat} = 0.010 \pm 0.001$ s^{-1}. However, it is not possible to determine steady state kinetic parameters for catalysis by D307A DCS and D311A DCS because the rate of δ-cadinene production is so low that it is beyond the capacity of the kinetic assays.

To probe the role of the second aspartate-rich motif $D^{451}DVAE^{455}$ on helix H that interacts with the putative Mg^{2+}_B ion, the D451A, D452A, and E455A mutants have been similarly produced and purified. While E455A DCS still generates δ-cadinene, it is not possible to determine steady state kinetic parameters for catalysis due to the very low activity of this mutant. In contrast, the steady state kinetic parameters for the cyclization of FPP by D451A DCS ($K_M = 2.4 \pm 0.3$ μM and $k_{cat} = 0.043 \pm 0.001$ s^{-1}) and D452A DCS ($K_M = 3.1 \pm 1.2$ μM and $k_{cat} = 0.014 \pm 0.001$ s^{-1}) are comparable to those measured for the wild-type enzyme.

Discussion

DCS contains a unique metal binding motif

Although DCS contains the aspartate-rich motif **D**DXX(**D**,**E**) (boldface residues coordinate metal ions) common to helix D of the terpenoid cyclases, it does not contain the NSE/DTE metal-binding motif common to helix H of the terpenoid cyclases usually occurring as **D**DXX**T**XXX**E** in plant cyclases (18,19,33,41,44,45). Instead, DCS contains a second aspartate-rich sequence $\mathbf{D}^{451}$DVA$\mathbf{E}^{455}$. Interestingly, the prenyltransferase farnesyl diphosphate synthase (FPPS) is an isoprenoid chain elongation enzyme rather than a cyclase, and this enzyme contains two conserved aspartate-rich DDXXD metal binding motifs. Peters has shown that the serine/threonine Mg^{2+}_B ligand in the NSE/DTE motif of certain plant cyclases is occasionally substituted by glycine, potentially allowing for an additional water molecule in the Mg^{2+}_B coordination polyhedron (20). Thus, the NSE/DTE motif for Mg^{2+}_B binding is not an absolutely universal signature sequence distinguishing a terpenoid cyclase from the greater family of terpenoid synthases such as FPPS. Curiously, FPPS is known to generate low levels of cyclic sesquiterpenoids (46), so the functional distinction between a cyclase and a chain elongation enzyme is likely to reside in the active site contour, i.e., the overall template for the reaction, and the carbon-carbon bond forming reactions permitted or prevented by this template.

Interestingly, mutations to the aspartate-rich motifs D^{307}DTYD^{311} and D^{451}DVAE^{455} of DCS, where each aspartate residue is individually replaced with alanine, do not completely obliterate catalytic activity. However, the D307A, D311A, and E455A substitutions severely compromise activity, which is consistent with the critical role of these residues in orienting the trinuclear magnesium cluster (Figure 3). In contrast, the D308A, D451A and D452A substitutions result in essentially unchanged turnover numbers. It is curious that the D451A substitution in the second aspartate-rich motif does not impact catalysis, since this residue interacts with the putative Mg^{2+}_B ion (Figure 3) and the corresponding aspartate does likewise in FPPS (22). Regardless, mutagenesis of E455 in DCS shows that the third carboxylate residue in the second aspartate-rich motif plays a significant role in metal binding and catalysis, whereas the corresponding residue in FPPS does not interact with Mg^{2+}_B. Therefore, subtle differences in metal binding interactions by conserved motifs can distinguish one terpenoid synthase from another.

Notably, while K_M for D308A DCS is increased 13-fold, it is largely unchanged for D451A DCS and D452A DCS. Mutagenesis experiments with other terpenoid synthases show that the second aspartate of the aspartate-rich motif can have a variable influence on catalytic activity (47-50). Presumably, such effects depend on the intramolecular interactions of the second aspartate residue in the enzyme-substrate complex. For example, the second aspartate residue in the aspartate-rich motifs of the fungal cyclases trichodiene synthase and aristolochene synthase engages in a salt link with an arginine residue to stabilize closed active site conformations (19,43). However, the side chain of D308 in DCS does not engage in hydrogen bond interactions in the crystal structures of unliganded DCS and its 2F-FPP complex.

When the trinuclear metal clusters of DCS, *A. terreus* aristolochene synthase (ATAS) (43), and *E. coli* FPPS (22) are compared, interesting similarities in metal ion interactions are observed despite the divergent evolution of the Mg^{2+}_B-binding motif (Figure 4). In the DCS-Mg^{2+}_3-2F-FPP complex, Mg^{2+}_B interacts with D451, E455, and one oxygen of the 2F-FPP diphosphate group. In the ATAS-Mg^{2+}_3-PP_i complex, Mg^{2+}_B is coordinated by E227, N219, S223, and two oxygen atoms of PP_i. Similarly, in the FPPS-Mg^{2+}_3-isopentenyl diphosphate-dimethylallyl-S-thiolodiphosphate complex, Mg^{2+}_B is coordinated by D244, two oxygen atoms of the isopentenyl diphosphate group, and three water molecules. Comparison of these structures reveals that when Mg^{2+}_B is coordinated by a DDXXD/E motif, the metal binding

residues are contained on a single, unbent helix H; when Mg^{2+}_B is coordinated by an NSE/DTE motif, a bend or an additional short helix (helix Hα-1) containing the serine/threonine and glutamate residues of the NSE/DTE motif is found at the C-terminal end of helix H. This conclusion also holds true for the structures of other terpenoid synthases determined in the presence of metal ions (19,33,41,43,44).

Concluding remarks

Based on the conformation of 2F-FPP in the active site and the proposed catalytic mechanism for DCS (Figure 1), the C10 and C1 atoms are too far apart (>6 Å) for the initial cyclization reaction to occur. This is a likely consequence of 2F-FPP binding in what appears to be a secondary isoprenoid binding site adjacent to the active site cleft of DCS (Figure 5). It is not clear whether this secondary isoprenoid binding site is important for catalysis. However, 2F-FPP appears to have a complex mode of inhibition (see Supporting Information, Figure S10), which could be consistent with the alternative mode of binding observed in the crystal structure.

Intermolecular interactions observed in the DCS active site nevertheless yield insight on metal coordination that is relevant to our understanding of catalysis. Although DCS contains a different motif for Mg^{2+}_B coordination, this cyclase shares a similar constellation of three Mg^{2+} ions for activating the substrate diphosphate group with other terpenoid cyclases such as 5-epi-aristolochene synthase (33), trichodiene synthase (19), limonene synthase (44), cineole synthase (45), aristolochene synthase (43,51), and bornyl diphosphate synthase (41). Accordingly, despite the divergent evolution of terpenoid synthases in all forms of life, the chemical strategy for the activation of isoprenoid diphosphate substrates with 3 metal ions is conserved and is also shared with isoprenoid elongation enzymes such as FPPS (22) and geranylgeranyl diphosphate synthase (52). The current study suggests that an aspartate-rich **D**DXX(X)**D/E** motif on helix H signals a single helix bearing potential Mg^{2+}_B ligands (boldface), and an NSE/DTE motif (**N, D**)D(L, I, V)X(**S, T**)XXX**E** signals a bend or an additional short helix (helix Hα-1) at the C-terminal end of helix H such that the first Mg^{2+}_B ligand in this motif (**N, D**) is on helix H, and the remaining Mg^{2+}_B ligands (**S, T**)XXX**E** are on the bend or on helix Hα-1 (Figure 4). We conclude that the distinction between an isoprenoid chain elongation enzyme and a cyclase is not necessarily rooted in the specific motifs for metal binding, but instead is rooted in the three-dimensional contour of the active site and the carbon-carbon bond forming reactions permitted or prevented by this template for catalysis.

Supplementary Material

Refer to Web version on PubMed Central for supplementary material.

Acknowledgement

We thank Dr Xiao-Ya Chen, Institute of Plant Physiology and Ecology, Shanghai Institutes for Biological Sciences Shanghai, China for plasmid pXC1 and Dr Susan E. Taylor for help with the early parts of this project. Data were collected at the Southeast Regional Collaborative Access Team (SER-CAT) beamline 22-ID-D at the Advanced Photon Source, Argonne National Laboratory. Supporting Institutions may be found at www.ser-cat.org/members.html. Data were also collected at the Northeastern Collaborative Access Team (NE-CAT) beamline 24-ID-C (supported by NIH grant RR15301) at the Advanced Photon Source, Argonne National Laboratory. Use of the Advanced Photon Source was supported by the U.S. Department of Energy, Office of Science, Office of Basic Energy Sciences, under Contract Numbers W-31-109-Eng-38 and DE-AC02-06CH11357.

References

1. Bell AA, Stipanovic RD, Howell CR, Fryxell PA. Antimicrobial terpenoids of *Gossypium*: hemigossypol, 6-methoxyhemigossypol and 6-deoxyhemigossypol. Phytochemistry 1975;14:225–231.

2. Bell, AA. Physiology of secondary products. In: Mauney, JR.; McD Stewart, J., editors. Cotton Physiology. The Cotton Foundation; Memphis, TN: 1986. p. 597-622.
3. Chappell J. The Biochemistry and molecular biology of isoprenoid metabolism. Plant Physiol 1995;107:1–6. [PubMed: 12228337]
4. Benedict CR, Alchanati I, Harvey PJ, Liu J, Stipanovic RD, Bell AA. The enzymatic formation of δ-cadinene from farnesyl diphosphate in extracts of cotton. Phytochemistry 1995;39:327–331.
5. Chen XY, Chen Y, Heinstein P, Davisson VJ. Cloning, expression, and characterization of (+)-delta-cadinene synthase: a catalyst for cotton phytoalexin biosynthesis. Arch. Biochem. Biophys 1995;324:255–266. [PubMed: 8554317]
6. Davis GD, Essenberg M. (+)-δ-Cadinene is a product of sesquiterpene cyclase activity in cotton. Phytochemistry 1995;39:553–567.
7. Davis EM, Tsuji J, Davis GD, Pierce ML, Essenberg M. Purification of (+)-delta-cadinene synthase, a sesquiterpene cyclase from bacteria-inoculated cotton foliar tissue. Phytochemistry 1996;41:1047–1055. [PubMed: 8728715]
8. Coutinho EM. Gossypol: a contraceptive for men. Contraception 2002;65:259–263. [PubMed: 12020773]
9. Cui GH, Xu ZL, Yang ZJ, Xu YY, Xue SP. A combined regimen of gossypol plus methyltestosterone and ethinylestradiol as a contraceptive induces germ cell apoptosis and expression of its related genes in rats. Contraception 2004;70:335–342. [PubMed: 15451339]
10. Band V, Hoffer AP, Band H, Rhinehardt AE, Knapp RC, Matlin SA, Anderson DJ. Antiproliferative effect of gossypol and its optical isomers on human reproductive cancer cell lines. Gynecol. Oncol 1989;32:273–277. [PubMed: 2920946]
11. Balci A, Sahin FI, Ekmekci A. Gossypol induced apoptosis in the human promyelocytic leukemia cell line HL 60. Tohoku J. Exp. Med 1999;189:51–57. [PubMed: 10622208]
12. Wang X, Wang J, Wong SC, Chow LS, Nicholls JM, Wong YC, Liu Y, Kwong DL, Sham JS, Tsa SW. Cytotoxic effect of gossypol on colon carcinoma cells. Life Sci 2000;67:2663–2671. [PubMed: 11105982]
13. Zhang M, Liu H, Guo R, Ling Y, Wu X, Li B, Roller PP, Wang S, Yang D. Molecular mechanism of gossypol-induced cell growth inhibition and cell death of HT-29 human colon carcinoma cells. Biochem. Pharmacol 2003;66:93–103. [PubMed: 12818369]
14. Benedict CR, Lu J-L, Pettigrew DW, Liu J, Stipanovic RD, Williams HJ. The cyclization of farnesyl diphosphate and nerolidyl diphosphate by a purified recombinant delta-cadinene synthase. Plant Physiol 2001;125:1754–1765. [PubMed: 11299356]
15. Yoshikuni Y, Martin VJJ, Ferrin TE, Keasling JD. Engineering cotton (+)-delta-cadinene synthase to an altered function: germacrene D-4-ol synthase. Chem. and Biol 2006;13:91–98. [PubMed: 16426975]
16. Lodewyk MW, Gutta P, Tantillo DJ. Computational studies on biosynthetic carbocation rearrangements leading to sativene, cyclosativene, α-ylangene, and β-ylangene. J. Org. Chem 2008;73:6570–6579. [PubMed: 18681400]
17. Steele CL, Crock J, Bohlmann J, Croteau R. Sesquiterpene synthases from grand fir (Abies grandis). Comparison of constitutive and wound-induced activities, and cDNA isolation, characterization, and bacterial expression of delta-selinene synthase and gamma-humulene synthase. J. Biol. Chem 1998;273:2078–2089. [PubMed: 9442047]
18. Cane DE, Kang I. Aristolochene synthase: purification, molecular cloning, high-level expression in *Escherichia coli*, and characterization of the *Aspergillus terreus* cyclase. Arch. Biochem. Biophys 2000;376:354–364. [PubMed: 10775423]
19. Rynkiewicz MJ, Cane DE, Christianson DW. Structure of trichodiene synthase from *Fusarium sporotrichioides* provides mechanistic inferences on the terpene cyclization cascade. Proc. Natl. Acad. Sci 2001;98:13543–13548. [PubMed: 11698643]
20. Zhou K, Peters RJ. Investigating the conservation pattern of a putative second terpene synthase divalent metal binding motif in plants. Phytochemistry 2009;70:366–369. [PubMed: 19201430]
21. Tarshis LC, Yan M, Poulter CD, Sacchettini JC. Crystal structure of recombinant farnesyl diphosphate synthase at 2.6 Å resolution. Biochemistry 1994;33:10871–10877. [PubMed: 8086404]

22. Hosfield DJ, Zhang Y, Dougan DR, Broun A, Tari LW, Swanson RV, Finn J. Structural basis for bisphosphonate-mediated inhibition of isoprenoid biosynthesis. J. Biol. Chem 2004;279:8526–8529. [PubMed: 14672944]
23. Kellogg BA, Poulter CD. Chain elongation in the isoprenoid biosynthetic pathway. Curr. Opin. Chem. Biol 1997;1:570–578. [PubMed: 9667899]
24. Lesburg CA, Caruthers JM, Paschall CM, Christianson DW. Managing and manipulating carbocations in biology: terpenoid cyclase structure and mechanism. Curr. Opin. Struct. Biol 1998;8:695–703. [PubMed: 9914250]
25. Wendt KU, Schulz GE. Isoprenoid biosynthesis: manifold chemistry catalyzed by similar enzymes. Structure 1998;6:127–133. [PubMed: 9519404]
26. Christianson DW. Structural biology and chemistry of the terpenoid cyclases. Chem. Rev 2006;106:3412–3442. [PubMed: 16895335]
27. Christianson DW. Unearthing the roots of the terpenome. Curr. Opin. Chem. Biol 2008;12:141–150. [PubMed: 18249199]
28. Shishova EY, Yu F, Miller DJ, Faraldos JA, Zhao Y, Coates RM, Allemann RK, Cane DE, Christianson DW. X-ray crystallographic studies of substrate binding to aristolochene synthase suggest a metal ion binding sequence for catalysis. J. Biol. Chem 2008;283:15431–15439. [PubMed: 18385128]
29. Miller DJ, Yu F, Allemann RK. Aristolochene synthase-catalyzed cyclization of 2-fluorofarnesyl-diphosphate to 2-fluorogermacrene A. ChemBioChem 2007;8:1819–1825. [PubMed: 17683054]
30. Calvert MJ, Ashton PR, Allemann RK. Germacrene A is a product of the aristolochene synthase-mediated conversion of farnesylpyrophosphate to aristolochene. J. Am. Chem. Soc 2002;124:11636–11641. [PubMed: 12296728]
31. Otwinowski Z, Minor W. Processing of X-ray diffraction data collected in oscillation mode. Methods Enzymol 1997;276:307–326.
32. McCoy AJ, Grosse-Kunstleve RW, Adams PD, Winn MD, Storoni LC, Read RJ. Phaser crystallographic software. J. Appl. Cryst 2007;40:658–674. [PubMed: 19461840]
33. Starks CM, Back K, Chappell J, Noel JP. Structural basis for cyclic terpene biosynthesis by tobacco 5-epi-aristolochene synthase. Science 1997;277:1815–1820. [PubMed: 9295271]
34. Brünger AT, Adams PD, Clore GM, DeLano WL, Gros P, Grosse-Kunstleve RW, Jiang J-S, Kuszewski J, Nilges M, Pannu NS, Read RJ, Rice LM, Simonson T, Warren GL. Crystallography & NMR system: a new software suite for macromolecular structure determination. Acta Crystallogr. D 1998;54:905–921. [PubMed: 9757107]
35. Jones TA, Zou J-Y, Cowan SW, Kjeldgaard M. Improved methods for building protein models in electron density maps and the location of errors in these models. Acta Crystallogr. A 1991;47:110–119. [PubMed: 2025413]
36. Emsley P, Cowtan K. Coot: model-building tools for molecular graphics. Acta Crystallogr 2004;D60:2126–2132.
37. Afonine PV, Grosse-Kunstleve RW, Adams PD. The Phenix refinement framework. CCP4 Newsletter 2005;42contribution 8
38. Laskowski RA, MacArthur MW, Moss DS, Thornton JM. PROCHECK: a program to check the stereochemical quality of protein structures. J. Appl. Cryst 1993;26:283–291.
39. Karp F, Zhao Y, Santhamma B, Assink B, Coates RM, Croteau RB. Inhibition of monoterpene cyclases by inert analogues of geranyl diphosphate and linalyl diphosphate. Arch. Biochem. Biophys 2007;468:140–146. [PubMed: 17949678]
40. Lesburg CA, Zhai G, Cane DE, Christianson DW. Crystal structure of pentalenene synthase: mechanistic insights on terpenoid cyclization reactions in biology. Science 1997;277:1820–1824. [PubMed: 9295272]
41. Whittington DA, Wise ML, Urbansky M, Coates RM, Croteau RB, Christianson DW. Bornyl diphosphate synthase: structure and strategy for carbocation manipulation by a terpenoid cyclase. Proc. Natl. Acad. Sci. USA 2002;99:15375–15380. [PubMed: 12432096]
42. Allemann RK. Chemical wizardry? The generation of chemical diversity in terpenoid biosynthesis. Pure Appl. Chem 2008;80:1773–1780.

43. Shishova EY, Di Costanzo L, Cane DE, Christianson DW. X-ray crystal structure of aristolochene synthase from *Aspergillus terreus* and evolution of templates for the cyclization of farnesyl diphosphate. Biochemistry 2007;46:1941–1951. [PubMed: 17261032]
44. Hyatt DC, Youn B, Zhao Y, Santhamma B, Coates RM, Croteau RB, Kang C. Structure of limonene synthase, a simple model for terpenoid cyclase catalysis. Proc. Natl. Acad. Sci. USA 2007;104:5360–5365. [PubMed: 17372193]
45. Kampranis SC, Ioannidis D, Purvis A, Mahrez W, Ninga E, Katerelos NA, Anssour S, Dunwell JM, Degenhart J, Makris AM, Goodenough PW, Johnson CB. Rational conversion of substrate and product specificity in a *Salvia* monoterpene synthase: structural insights into the evolution of terpene synthase function. Plant Cell 2007;19:1994–2005. [PubMed: 17557809]
46. Saito A, Rilling HC. The formation of cyclic sesquiterpenes from farnesyl pyrophosphate by prenyltransferase. Arch. Biochem. Biophys 1980;208:508–511. [PubMed: 7259201]
47. Felicetti B, Cane D. Aristolochene synthase: mechanistic analysis of active site residues by site-directed mutagenesis. J. Am. Chem. Soc 2004;126:7212–7221. [PubMed: 15186158]
48. Song L, Poulter CD. Yeast farnesyl-diphosphate synthase: site-directed mutagenesis of residues in highly conserved prenyltransferase domains I and II. Proc. Natl. Acad. Sci. USA 1994;91:3044–3048. [PubMed: 8159703]
49. Cane DE, Xue Q, Fitzsimons BC. Trichodiene synthase. Probing the role of the highly conserved aspartate-rich region by site-directed mutagenesis. Biochemistry 1996;35:12369–12376. [PubMed: 8823172]
50. Seemann M, Zhai G, de Kraker J-W, Paschall CM, Christianson DW, Cane DE. Pentalenene synthase. Analysis of active site residues by site-directed mutagenesis. J. Am. Chem. Soc 2002;124:7681–7689. [PubMed: 12083921]
51. Caruthers JM, Kang I, Rynkiewicz MJ, Cane DE, Christianson DW. Crystal structure determination of aristolochene synthase from the blue cheese mold, *Penicillium roqueforti*. J. Biol. Chem 2000;275:25533–25539. [PubMed: 10825154]
52. Kloer DP, Welsch R, Beyer P, Schulz GE. Structure and reaction geometry of geranylgeranyl diphosphate synthase from *Sinapis alba*. Biochemistry 2006;45:15197–15204. [PubMed: 17176041]

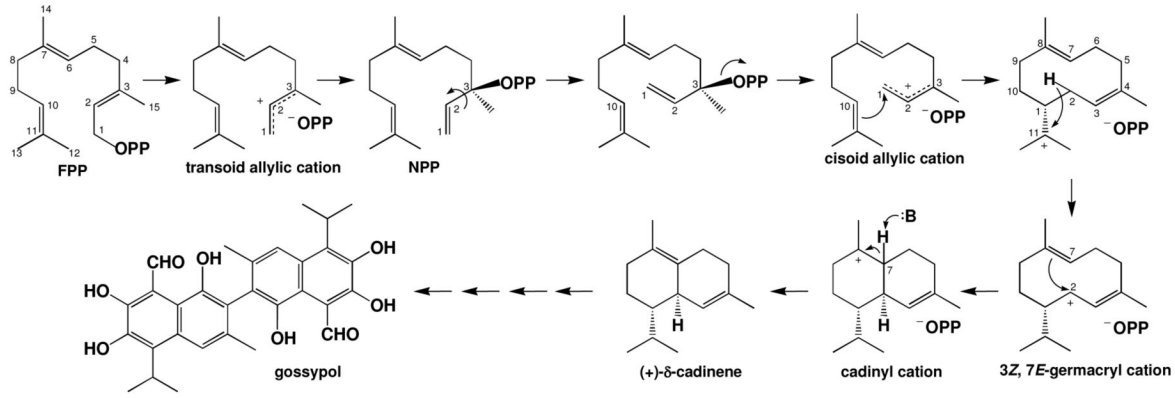

Figure 1.

Proposed catalytic mechanism for (+)-δ-cadinene synthase from *Gossypium arboreum* (15). The reaction is initiated by ionization and isomerization of farnesyl diphosphate (FPP) to yield nerolidyl diphosphate (NPP), which undergoes rotation about the C2-C3 bond and reionization to yield a cisoid allylic cation. Cyclization is achieved by C1-C10 bond formation, which is followed by a 1,3 hydride shift from C2 to C11 to form the 3*Z*, 7*E*-germacryl cation. Subsequent C7-C2 bond formation yields the cadinyl cation, which undergoes proton abstraction at C7 to generate (+)-δ-cadinene. While the identity of the base (B:) in the final step is not known, it is possible that the pyrophosphate leaving group ($^{-}$OPP, which represents $PO_4PO_3^{4-}$) serves this function, as proposed in the mechanisms of aristolochene synthase (43,51) and farnesyl diphosphate synthase (22). Further oxidation and coupling steps yield gossypol.

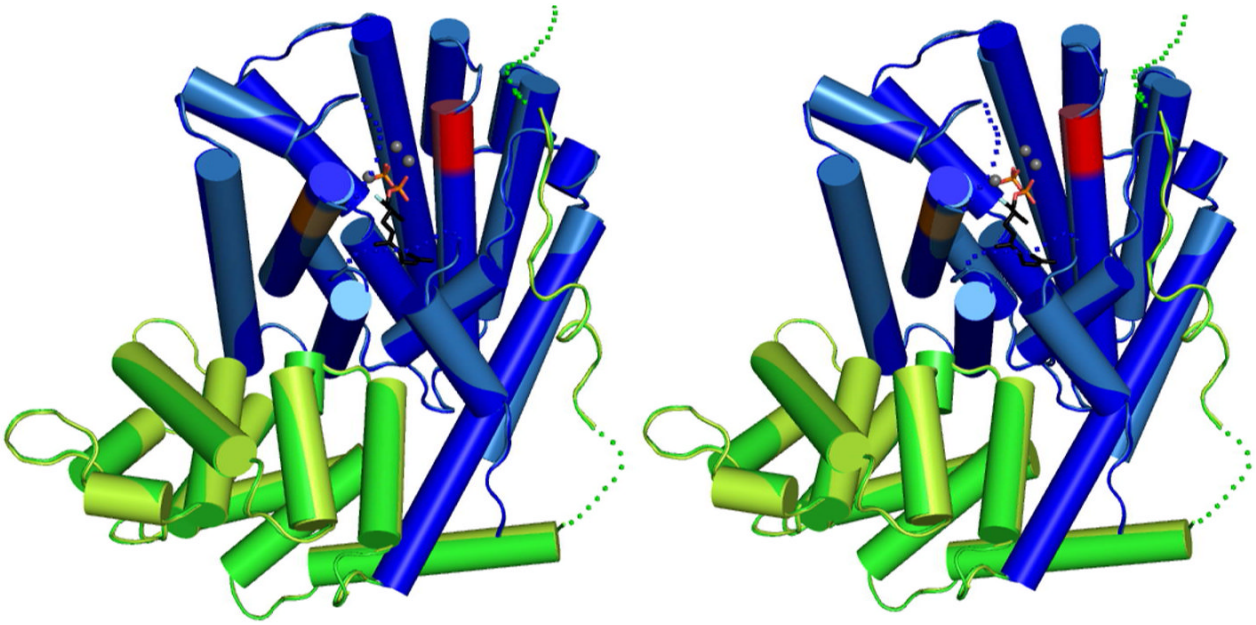

Figure 2.

The C-terminal catalytic domain of DCS adopts the α-helical class I terpenoid synthase fold (unliganded DCS, blue; 2F-FPP complex, light blue), and the non-catalytic N-terminal domain adopts an α-helical fold similar to that of a class II terpenoid synthase (unliganded DCS, green; 2F-FPP complex, light green). In the catalytic domain, the aspartate-rich $D^{307}DTYD^{311}$ metal-binding motif on helix D is red and the second metal-binding motif $D^{451}DVAE^{455}$ on helix H is orange. Disordered polypeptide segments are indicated by dotted lines. Putative Mg^{2+} ions are shown as small gray spheres. For 2F-FPP, atoms are color-coded as follows: C = black, O = red, P = orange, and F = light blue.

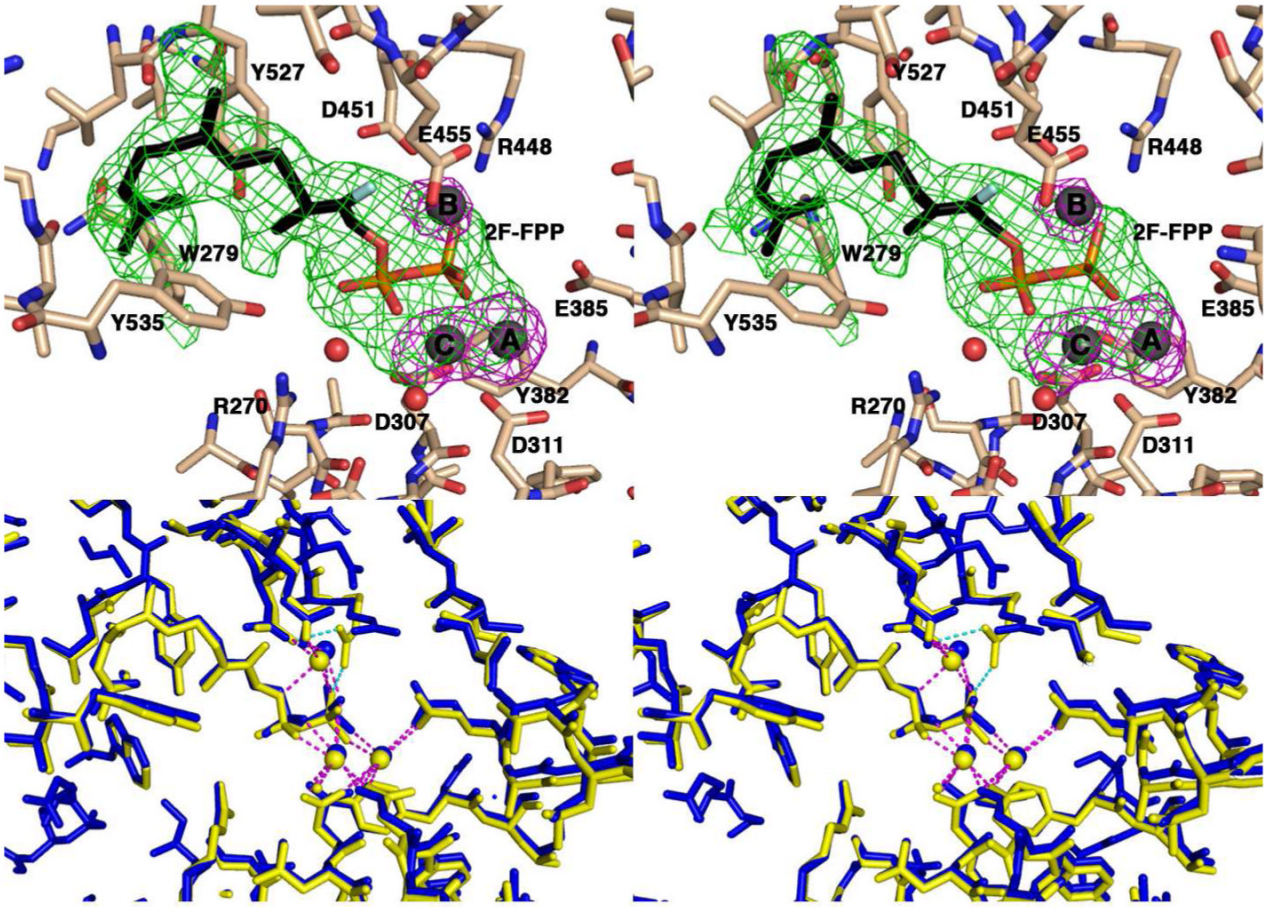

Figure 3.

(a) Simulated annealing omit maps of 2F-FPP (green, contoured at 3.5 σ) and putative Mg^{2+} ions (magenta, contoured at 4.0 σ) in monomer A of the DCS-2F-FPP complex. Selected active site residues are indicated and atoms are color-coded as follows: C = tan (DCS) or black (2F-FPP), O = red, N = blue, P = orange, S = green, and F = cyan; putative Mg^{2+} ions appear as gray spheres and water molecules appear as red spheres. (b) Stereoview of the superposition of monomer A (yellow) and monomer B (blue) of the DCS-2F-FPP complex shows that isoprenoid binding is generally similar in both monomers. Dashed lines represent Mg^{2+} (magenta) and hydrogen bond (green) interactions.

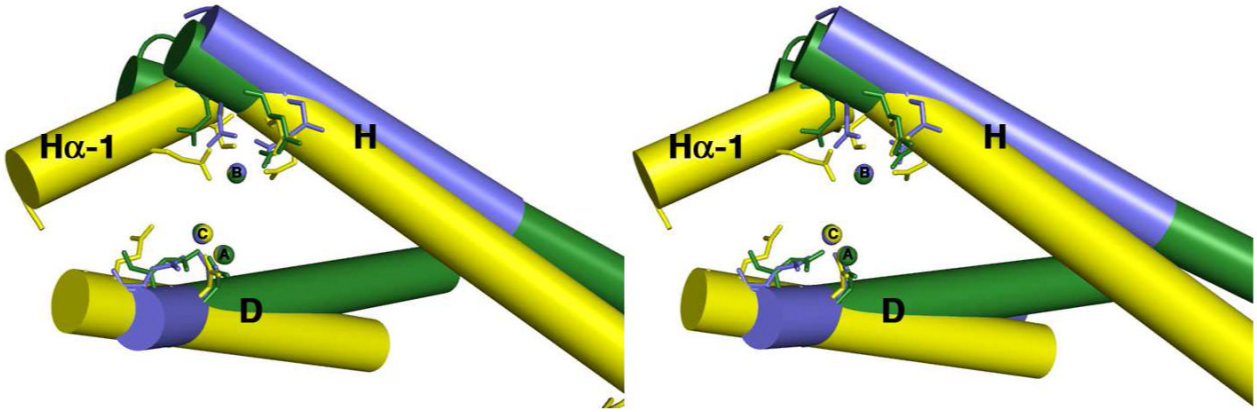

Figure 4.

Superposition of helices D and H of *A. terreus* aristolochene synthase complexed with PP_i (yellow), *E. coli* farnesyl diphosphate synthase complexed with isopentenyl diphosphate and dimethylallyl S-thiolodiphosphate (green), and DCS complexed with 2F-FPP (blue), based on the superposition of their trinuclear metal clusters. For clarity, only residues interacting with Mg^{2+}_A, Mg^{2+}_B, and Mg^{2+}_C are shown on helices D, H, and Hα-1. The constellation of three magnesium ions is identical regardless of whether Mg^{2+}_B is chelated by an aspartate-rich motif or the NSE/DTE motif, and regardless of whether the enzyme catalyzes an isoprenoid chain elongation reaction or a cyclization reaction. Coordination of Mg^{2+}_B by an NSE/DTE motif requires the additional helix Hα-1.

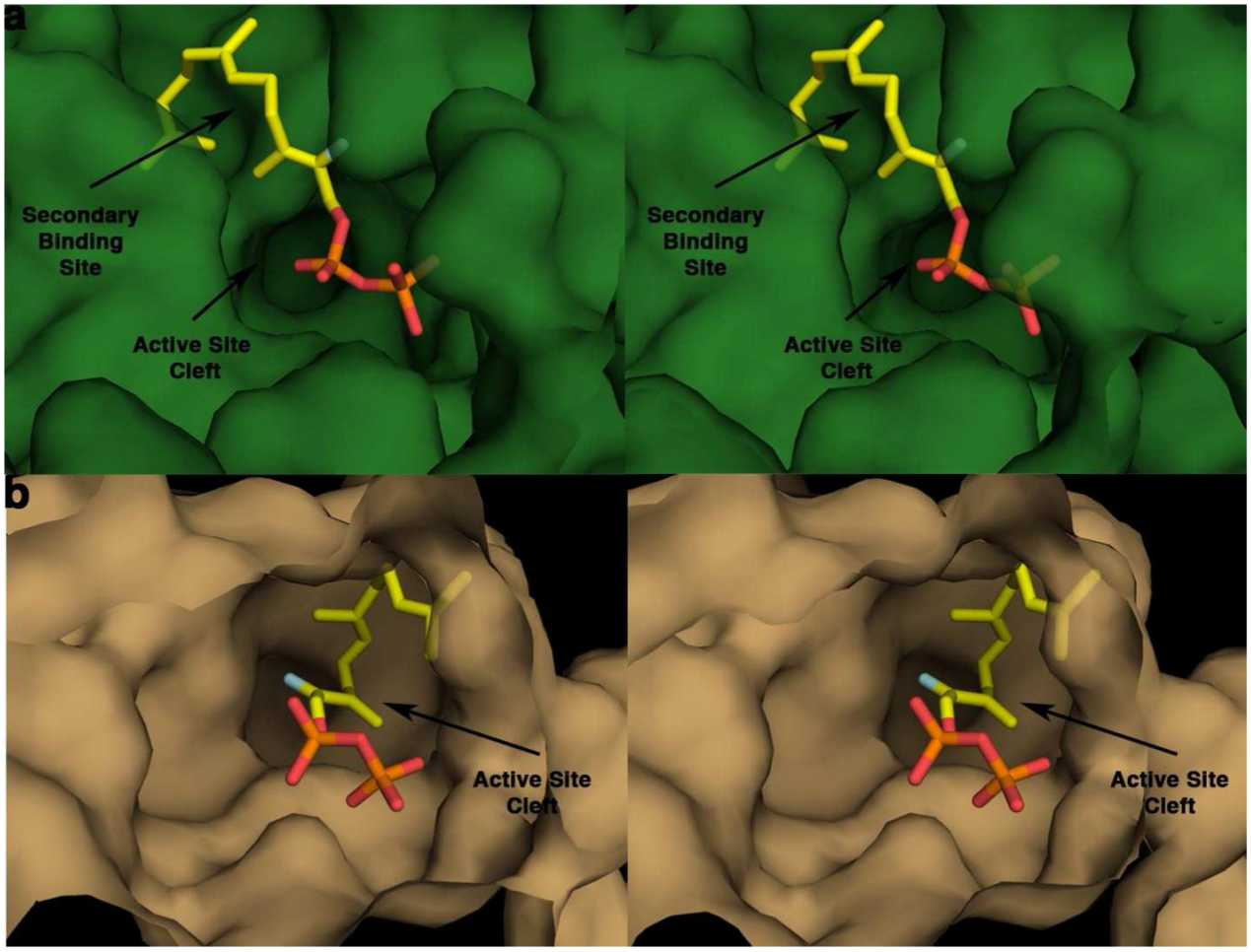

Figure 5.
Stereoviews of active site contours of DCS (a) and *A. terreus* aristolochene synthase (b) looking into the ~18 Å deep active site clefts. The isoprenoid moiety of the substrate analogue 2F-FPP binds in a secondary cleft adjacent to the main active site cleft of DCS. In contrast, the isoprenoid moiety of 2F-FPP binds in the main active site cleft of aristolochene synthase (28).

Table 1

Data Collection and Refinement Statistics

Structure	Unliganded DCS	DCS-2F-FPP
Resolution range (Å)	50.0-2.40	50-2.75
Reflections (measured/ unique)	98790/51262	130161/34661
Completeness (%) (overall/ outer shell)	99.4/100.0	99.9/99.9
R_{merge} [a] (overall/outer shell)	0.099/0.460	0.083/0.487
<I/σ> (overall/outer shell)	19.8/4.7	13.0/3.2
Protein atoms (no.) [b]	8390	8402
Solvent atoms (no.) [b]	380	177
Metal ions (no.) [b]	0	6
Ligand atoms (no.) [b]	0	50
Refinement		
Reflections used in refinement (work/free)	51193/2040	34635/1708
R/R_{free} [c]	0.187/0.239	0.201/0.256
Average B factors (Å^2)		
Protein main chain atoms	54	66
Protein side chain atoms	78	68
2F-FPP	---	84
Mg^{2+} ions	---	58
β-Mercaptoethanol	78	72
Glycerol	84	---
Water molecules	58	58
R.m.s. deviations		
bonds (Å)	0.010	0.010
angles (deg.)	1.2	1.3
Dihedral angles (deg.)	18.4	21.4
Ramachandran plot		
Most favored regions (%)	91.8	90.1
Additionally allowed (%)	7.2	8.9
Generously allowed (%)	0.9	1.0
Disallowed (%)	0.1	0

[a] $R_{merge} = \Sigma|I_j - \langle I_j \rangle| / \Sigma I_j$, where I_j is the observed intensity for reflection j and $\langle I_j \rangle$ is the average intensity calculated for reflection j from replicate data.

[b] Per asymmetric unit.

[c] $R = \Sigma||F_O| - |F_C|| / \Sigma F_O$, where R and R_{free} are calculated using the working and test reflection sets, respectively.